Downloaded from jnm.snmjournals.org by on March 13, 2017. For personal use only.

Internal Pair Production of ^{90}Y Permits Hepatic Localization of Microspheres Using Routine PET: Proof of Concept

Vanessa L. Gates[1], Abdulredha A.H. Esmail[2], Karen Marshall[3], Stewart Spies[1], and Riad Salem[3]

[1]Section of Nuclear Medicine, Department of Radiology, Northwestern University, Chicago Illinois; [2]Department of Nuclear Medicine, Faisal Sultan Bin Issa Center for Diagnosis and Radiation Therapy, Kuwait Cancer Control Center, Sabah Health District, Kuwait; and [3]Section of Interventional Radiology, Department of Radiology, Robert H. Lurie Comprehensive Cancer Center, Northwestern University, Chicago, Illinois

Radioembolization with ^{90}Y microspheres represents a novel transarterial radiation treatment for liver tumors. The purpose of this pilot study was to evaluate the findings of postimplantation PET/CT of ^{90}Y glass microspheres. **Methods:** Three patients with hepatocellular carcinoma and 2 patients with liver metastases (1 neuroendocrine, 1 colorectal) underwent PET/CT after radioembolization. Four patients underwent imaging at 1 mo to assess response and confirm PET/CT findings; 1 patient underwent PET/CT at 4 d after ^{90}Y implantation. Patients were followed for adverse events. **Results:** Standard PET/CT enabled the localization of ^{90}Y glass microspheres for all patients. None of the patients experienced adverse events related to nontarget deposition. **Conclusion:** Standard PET/CT may be used to assess the localization of ^{90}Y glass microspheres. This approach provides a simple, rapid, and universally applicable method of confirming microsphere deposition. With further validation, this technique may potentially become the standard of care for confirming microsphere distribution.

Key Words: hepatocellular carcinoma; radiotherapy; radioembolization; ^{90}Y microspheres; PET/CT; bremsstrahlung

J Nucl Med 2011; 52:72–76
DOI: 10.2967/jnumed.110.080986

The tracer ^{90}Y is traditionally thought of as a pure β-emitter. Thus, current clinical practice involves determining the distribution of the microspheres through bremsstrahlung imaging combined with anatomic imaging via SPECT/CT (*1*). Because bremsstrahlung imaging is based on a SPECT acquisition that uses either a wide imaging window or multiple energy windows due to the continuum, the scattered photon cannot easily be distinguished from true photons. Consequently, bremsstrahlung imaging is not quantifiable, and thus accurate dose distribution cannot be obtained (*2*).

Received Jul. 26, 2010; revision accepted Oct. 7, 2010.
For correspondence or reprints contact: Riad Salem, Section of Interventional Radiology, Department of Radiology, Robert H. Lurie Comprehensive Cancer Center, Northwestern University, 676 N. St. Clair, Ste. 800, Chicago, IL 60611.
E-mail: r-salem@northwestern.edu
COPYRIGHT © 2011 by the Society of Nuclear Medicine, Inc.

In an effort to improve pretreatment evaluation and follow-up, microspheres containing radionuclides that emit both β- and γ-radiations have been proposed, and treatment with microspheres includes the use of ^{166}Ho and ^{186}Re/^{188}Re. At the time of this article's publication, glass and poly (L-lactic acid) (PLLA) microspheres incorporating ^{186}Re/^{188}Re had not been tested in human subjects with liver tumors. However, ^{188}Re human serum albumin microspheres (^{188}Re-HSAM) have been tested in a small cohort of patients at a single institution (*3*). The maximum β-particle energy of ^{188}Re (2.12 MeV) is lower than that of ^{90}Y (2.28 MeV), thus necessitating 4- to 5-fold-higher activities to obtain an absorbed dose equivalent to that of ^{90}Y. Because the γ-energy (155 keV) is comparable to other nuclear medicine imaging agents, ^{188}Re-HSAM seems to be a good candidate for radioembolization of liver tumors. However, no conclusive effects could be derived from the study performed by Liepe et al. because of the small cohort size and heterogeneity of the patients' primary disease (*3*). To properly evaluate the effect of radioembolization of hepatic malignancies with ^{188}Re-HSAM, more studies and a larger patient cohort are warranted.

Another promising radionuclide proposed for radioembolization of hepatic tumors is ^{166}Ho (maximum energy of the β-particle, 1.77 [48.7%] and 1.85 [50.5%] MeV and energy of the γ-ray, 81 keV [6.7%]). ^{166}Ho PLLA microspheres are currently being used in patients with hepatic malignancies under a phase I clinical trial (*4,5*). Similar to the ^{188}Re HSAM dosimetry, the absorbed radiation dose per activity of ^{166}Ho (8.7 mGy/MBq) is lower than that of ^{90}Y (28 mGy/MBq). As a result, with ^{166}Ho 3 times the radioactivity will be required for radioembolization to achieve a dosimetry equivalent to that of ^{90}Y. The greatest advantage of ^{166}Ho is that it represents a multimodality imaging agent (*6*). The paramagnetic properties of ^{166}Ho allow ^{166}Ho PLLA to show a high transverse relaxation rate that is visualized as dark regions on a T2*-weighted MR image (*7*). Moreover, the ^{166}Ho x-ray attenuation coefficient is sufficiently high enough to be used as a contrast agent for visualization through CT (*6*). The greatest disadvantage of ^{166}Ho PLLA is the relatively short half-life of the tracer, meaning that each dose will require separate

Downloaded from jnm.snmjournals.org by on March 13, 2017. For personal use only.

TABLE 1
Primary Disease, Location of Microcatheter Tip in Hepatic Artery, and Administered Radioactivity of ^{90}Y Glass Microspheres for Each Patient

Patient	Primary disease	Location of administration site	^{90}Y glass microspheres administered radioactivity (GBq)
1	HCC	Superior lateral left hepatic artery	1.29
2	HCC	Segment A of middle hepatic artery	2.08
3	Metastatic colorectal carcinoma	Lobar right hepatic artery	2.68
4	HCC	Inferior segment of posterior right hepatic artery	1.33
5	Metastatic neuroendocrine disease	Lobar right hepatic artery	10.52

neutron irradiation and a short logistic timeline to get the dose from the reactor to the patient (*8*).

However, for ^{90}Y the internal pair production (positron) branching ratio for the 0+–0+ transition of ^{90}Zr from ^{90}Y, determined by Selwyn et al. to be $31.867 \pm 0.47 \times 10^{-6}$, does allow for the possibility of using coincidence imaging (*9*). Nickles et al. showed that it was possible to qualitatively assess the distribution of ^{90}Y using PET (*10*). Although Nickles et al. demonstrated excellent resolution of 2 syringes filled with less than 37 MBq of ^{90}Y, the images were obtained from an overnight scan, challenging the clinical applicability of this method (*10*). More recently, Lhommel et al. have published an ^{90}Y time-of-flight PET study that demonstrated with high resolution the biodistribution of ^{90}Y-labeled resin microspheres within a female patient with colorectal liver metastases (*11*). Unfortunately, time-of-flight PET/CT is not commonly available for many institutions performing radioembolization; alternatively, standard PET/CT is more easily accessible. Consequently, we postulated that standard PET/CT would successfully assess the biodistribution of ^{90}Y glass microspheres (TheraSphere; MDS Nordion) that were administered for the treatment of hepatic tumors.

MATERIALS AND METHODS

Patient Sample

Three patients with hepatocellular carcinoma (HCC) and 2 patients with liver metastases underwent dedicated whole-body PET/CT after radioembolization for their liver tumors. The technical details for radioembolization have been discussed in detail elsewhere (*12*). Briefly, all patients underwent pretreatment diagnostic angiography with ^{99m}Tc-labeled macroaggregated albumin (^{99m}Tc-MAA). Subsequently, all were treated with ^{90}Y glass microspheres and underwent immediate post–^{90}Y implantation PET/CT within 2 h of treatment. Our institution does not require review board approval for case reports. The activity administered and location of injection for each patient are described in Table 1.

Diagnostic Arterial Imaging

As part of the routine diagnostic work-up for radioembolization, all patients were administered approximately 74 MBq of ^{99m}Tc-MAA via a microcatheter positioned in a branch of the hepatic artery at 2 wk before treatment. Arterial distribution of the particles was quantified from SPECT/CT fused images that were obtained on the Siemens Symbia T (SPECT/CT) scanner using a 128×128 acquisition matrix with 60 frames (angular step, 3°) at a rate of 35 s per frame. Attenuation correction was achieved through the CT acquisition (130 kV, 25 mAs, B30 kernel, and 5-mm slices). Reconstructed images were fused and analyzed with Syngo TrueD (2008 version; Siemens AG).

Immediate Posttreatment ^{90}Y PET/CT Acquisition Parameters

On the day of treatment with ^{90}Y, dedicated whole-body PET/CT scans from the chest to just above the pelvis were obtained using the Biograph 40 with Pico-3D, Hi-REZ, and TrueV options (Siemens Medical Solutions USA, Inc.), within 2 h after intraarterial adminis-

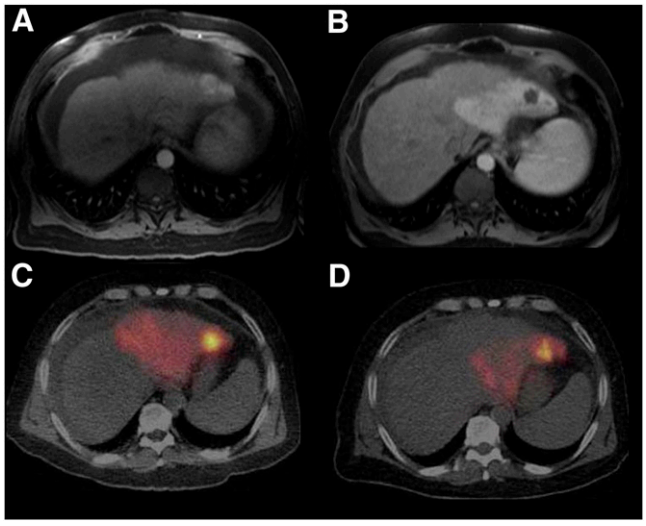

FIGURE 1. (A) Hypervascular tumors are noted on pretreatment MR image of 68-y-old man diagnosed with HCC. (C) SPECT/CT image (74 MBq of ^{99m}Tc-MAA was administered via microcatheter placed in left hepatic artery) shows increased activity deposition in superior lateral left hepatic artery. (B) One-month posttreatment MR image demonstrates absence of tissue enhancement, suggesting complete tumor necrosis, and normal parenchyma radiation effect in superior lateral left hepatic artery. (D) Immediate posttreatment (1.29 GBq of ^{90}Y administered via catheter placed in superior lateral left hepatic artery) PET/CT activity distribution matches the 1-mo posttreatment MR image region with the radiation effect.

Downloaded from jnm.snmjournals.org by on March 13, 2017. For personal use only.

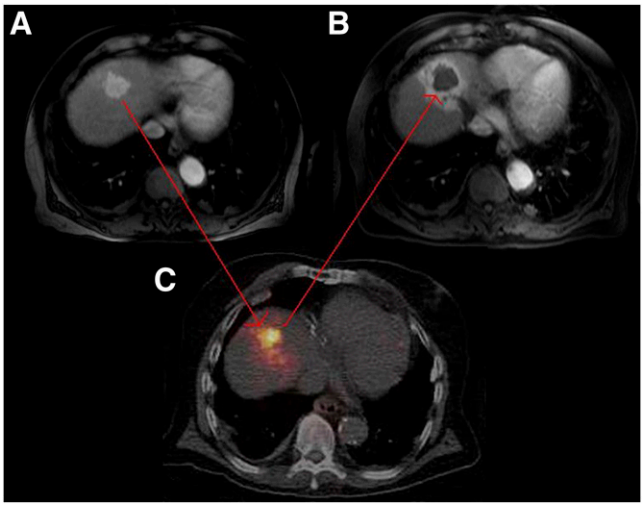

FIGURE 2. (A) Middle hepatic lobe hypervascular tumor noted on pretreatment MR image of 73-y-old man diagnosed with HCC. (B) One-month posttreatment MR image demonstrates absence of tissue enhancement, suggesting complete tumor necrosis, and normal parenchyma radiation effect. (C) Immediate posttreatment (2.08 GBq of ^{90}Y administered via catheter placed in middle hepatic artery) PET/CT activity distribution matches 1-mo posttreatment MR image region with radiation effect.

tration of ^{90}Y glass microspheres. The PET component consisted of 52 detector rings, with a total of 21,448 cerium-doped lutetium orthosilicate (LSO) crystal detectors (4.00 × 4.00 × 20 mm). The coincidence time resolution was 500 ps, and the sensitivity was

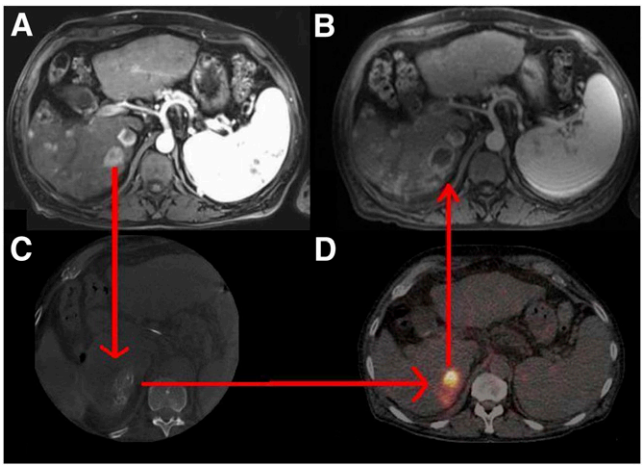

FIGURE 3. (A) Right hepatic segment 6 hypervascular tumor noted on contrast-enhanced pretreatment MR image of 64-y-old man diagnosed with HCC. (C) Dyna-CT, with contrast administered via microcatheter placed in segment 6 artery off posterior right hepatic artery, shows increased contrast distribution, suggesting hypervascular tumor. (B) One-month posttreatment MR image demonstrates absence of tissue enhancement, suggesting complete tumor necrosis, and normal parenchyma radiation effect. (D) Immediate posttreatment (1.33 GBq of ^{90}Y administered via catheter placed in inferior segmental branch off posterior right hepatic artery) PET/CT activity distribution matches 1-mo posttreatment MR image region with radiation effect.

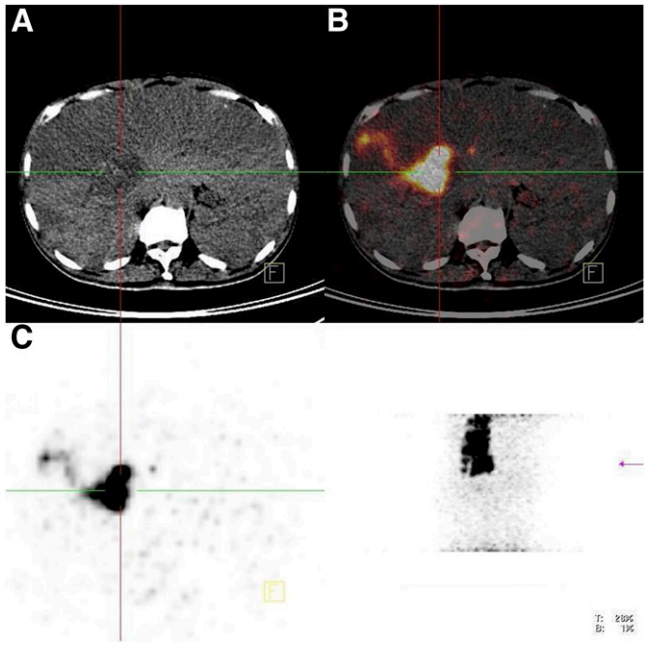

FIGURE 4. Unenhanced CT (A), fused PET/CT (C), and PET (B) images of man diagnosed with metastatic neuroendocrine disease. Images were obtained at 4 d after treatment (10.52 GBq of ^{90}Y glass microspheres were administered via catheter placed in right hepatic artery).

approximately 8.4 cps/kBq. The volumetric resolution was approximately 40 mm^3 at 10 cm. The CT component was a Sensation S-B40 (Siemens Medical Solutions), which had an average cross-field uniformity of ±2 *Hounsfield units* in a 20-cm water phantom position near the center of rotation.

All patients were positioned on the imaging table with their arms elevated. After the imaging field had been determined with an initial scout scan, an 80- to 110-s whole-body CT scan was acquired using the following parameters: 120 kVp, 40 mA, 1-s tube rotation, 4-mm slice collimation, and an 8-mm/s (i.e., pitch, 2) bed speed. On completion of the CT portion, the PET emission data were acquired for 10 min/bed position for all patients. Imaging included 2 bed positions per patient, with the liver centered between the 2 positions, resulting in whole-body PET emission durations of 20 min. No effort was made to prevent saturation of the detectors from bremsstrahlung x-rays or reduce the noise generated from the LSO crystal.

^{90}Y PET/CT Tomographic Reconstruction Parameters

Tomographic images were generated by iterative reconstruction with segmented attenuation correction using the following parameters for the Siemens Biograph 40: True-X; subset, 21; iteration, 3; matrix, 168 × 168; postprocessing filter, 4 mm in full width at half maximum; loop filter, 4 mm in full width at half maximum; and gaussian smooth filter, 4 mm. PET images were analyzed by visual inspection of hepatic metastases using Syngo TrueD. Although the activity distribution could not be derived from these initial images, the tumor–to–normal tissue average counts (TN) were assessed from a volume region of interest drawn on the PET/CT images and compared with a TN obtained from the SPECT/CT images of the ^{99m}Tc-MAA distribution in 2 cases.

Downloaded from jnm.snmjournals.org by on March 13, 2017. For personal use only.

TABLE 2
TN Results from 2 Patients

Patient	Diagnostic microcatheter hepatic artery placement	SPECT/CT TN	Treatment microcatheter hepatic artery placement	^{90}Y administered activity (GBq)	PET/CT TN
1	Left	7	Superior lateral left	1.29	6.3
3	Right	5.1	Right	2.68	7.4

RESULTS

Patients

All patients underwent successful treatment without any reportable or recordable medical events. In the 4 patients with imaging follow-up at 1 mo, treatment effect was confirmed. In the 3 patients with HCC, the absence of contrast enhancement suggested complete tumor necrosis. In the patient with metastatic colorectal cancer, carcinoembryonic antigen decreased from 18 to 5, with the posttreatment CT scan confirming decreased tumoral contrast enhancement and size.

Figures 1–4 represent 4 different patients for whom PET/CT images show an area of increased activity reflecting the biodistribution of ^{90}Y glass. As is illustrated with diagnostic imaging such as Dyna CT or intraarterially administered ^{99m}Tc-MAA SPECT/CT, the ^{90}Y glass microsphere radioactivity is preferentially deposited in the tumor. This is quantitatively illustrated by comparing the TN for 2 patients who had similar microcatheter positions for both the ^{99m}Tc-MAA SPECT/CT study and the ^{90}Y PET/CT study (Table 2).

Imaging Technique

Imaging time for all cases was less than 20 min. Because this was a proof of concept analysis, longer acquisition times for possible statistical quantitative data were not explored. The maximum true coincidence counting rate ranged from approximately 124 cps (patient 1) to 308 cps (patient 3). These counting rates are similar to those reported by Nickles et al. (*10*).

Adverse Events

There are important reasons for microsphere imaging: to confirm microsphere deposition, predict a tumor response, prevent or mitigate adverse events, and potentially determine TN ratio. This last concept may result in a significant improvement of dosimetry associated with microspheres. None of the 5 patients experienced adverse events related to nontarget deposition, as was consistent with the ^{90}Y PET images.

DISCUSSION

On the basis of our pilot study, standard PET/CT using LSO scintillation detectors may be used to assess the biodistribution of ^{90}Y glass microspheres. Our experience suggests that measures reducing signal-to-noise ratio, such as the use of copper shielding or time-of-flight imaging systems, were not required. We obtained TN values that were comparable to the values obtained from the diagnostic arterial studies. Unfortunately, the lutetium element of the crystal contains a trace amount of a naturally long decaying radioactive isotope (^{176}Lu), which will provide some background counting rate that needs to be corrected before any quantitative assessment is performed.

Imaging patients who have been administered ^{90}Y glass microspheres using a PET/CT system has the potential to greatly improve treatment planning by confirming the biodistribution of the microspheres with a resolution range of 2.5–4 mm. Physicians may be able to improve treatment outcomes using the PET/CT image to determine alternative supplying vessels, thus providing better tumor coverage. Although the inaccuracies and quantification techniques appear to be a work in progress, microsphere localization may prove to be a more relevant acute need, because this therapy, without partition modeling, has been shown to be safe.

CONCLUSION

This wider availability of the microsphere imaging technique should contribute to the better understanding of the distribution of microspheres used for radioembolization of hepatic tumors. With the resolution gain from PET/CT and thus the improved accuracy of the dose distribution, future patient treatment outcomes may be improved and patient-specific dosimetric methodologies may be achievable. However, the clearest message from our pilot study appears to be that ^{90}Y microspheres can be visualized with a simple 20-min PET/CT scan acquired using universally available technology. Postimplantation distribution can now be easily confirmed.

REFERENCES

1. Mansberg R, Sorensen N, Mansberg V, Van der Wall H. Yttrium 90 bremsstrahlung SPECT/CT scan demonstrating areas of tracer/tumour uptake. *Eur J Nucl Med Mol Imaging.* 2007;34:1887.
2. Sandström M, Lubberink M, Lundquist H. Quantitative SPECT with yttrium-90 for radionuclide therapy dosimetry. *Eur J Nucl Med Mol Imaging.* 2007;32:S260.
3. Liepe K, Brogsitter C, Leonhard J, et al. Feasibility of high activity rhenium-188-microsphere in hepatic radioembolization. *Jpn J Clin Oncol.* 2007;37:942–950.
4. Bult W, Vente MA, Zonnenberg BA, Van Het Schip AD, Nijsen JF. Microsphere radioembolization of liver malignancies: current developments. *Q J Nucl Med Mol Imaging.* 2009;53:325–335.
5. Smits ML, Nijsen JF, van den Bosch MA, et al. Holmium-166 radioembolization for the treatment of patients with liver metastases: design of the phase I HEPAR trial. *J Exp Clin Cancer Res.* 2010;29:70.
6. Vente MA, de Wit TC, van den Bosch MA, et al. Holmium-166 poly(L-lactic acid) microsphere radioembolisation of the liver: technical aspects studied in a large animal model. *Eur Radiol.* 2010;20:862–869.

Downloaded from jnm.snmjournals.org by on March 13, 2017. For personal use only.

7. Seevinck PR, Seppenwoolde JH, Zwanenburg JJ, Nijsen JF, Bakker CJ. FID sampling superior to spin-echo sampling for T2*-based quantification of holmium-loaded microspheres: theory and experiment. *Magn Reson Med.* 2008;60:1466–1476.
8. Vente MA, Nijsen JF, de Roos R, et al. Neutron activation of holmium poly(L-lactic acid) microspheres for hepatic arterial radio-embolization: a validation study. *Biomed Microdevices.* 2009;11:763–772.
9. Selwyn RG, Nickles RJ, Thomadsen BR, DeWerd LA, Micka JA. A new internal pair production branching ratio of ^{90}Y: the development of a non-destructive assay for ^{90}Y and 90Sr. *Appl Radiat Isot.* 2007;65:318–327.
10. Nickles RJ, Roberts AD, Nye JA, Converse AK, Barnhart TE, Avila-Rodriguez MA. Assaying and PET imaging of yttrium-90: 1>>34 ppm>0. *IEEE Nucl Sci Symp Rec.* 2004;6:3412–3414.
11. Lhommel R, Goffette P, Van den Eynde M, et al. Yttrium-90 TOF PET scan demonstrates high-resolution biodistribution after liver SIRT. *Eur J Nucl Med Mol Imaging.* 2009;36:1696.
12. Salem R, Thurston KG. Radioembolization with ^{90}Yttrium microspheres: a state-of-the-art brachytherapy treatment for primary and secondary liver malignancies—Part 1: Technical and methodologic considerations. *J Vasc Interv Radiol.* 2006;17:1251–1278.

Downloaded from jnm.snmjournals.org by on March 13, 2017. For personal use only.

JNM The Journal of NUCLEAR MEDICINE

Internal Pair Production of ^{90}Y Permits Hepatic Localization of Microspheres Using Routine PET: Proof of Concept

Vanessa L. Gates, Abdulredha A.H. Esmail, Karen Marshall, Stewart Spies and Riad Salem

J Nucl Med. 2011;52:72-76.
Published online: December 13, 2010.
Doi: 10.2967/jnumed.110.080986

This article and updated information are available at:
http://jnm.snmjournals.org/content/52/1/72

Information about reproducing figures, tables, or other portions of this article can be found online at:
http://jnm.snmjournals.org/site/misc/permission.xhtml

Information about subscriptions to JNM can be found at:
http://jnm.snmjournals.org/site/subscriptions/online.xhtml

The Journal of Nuclear Medicine is published monthly.
SNMMI | Society of Nuclear Medicine and Molecular Imaging
1850 Samuel Morse Drive, Reston, VA 20190.
(Print ISSN: 0161-5505, Online ISSN: 2159-662X)

© Copyright 2011 SNMMI; all rights reserved.

SNMMI SOCIETY OF NUCLEAR MEDICINE AND MOLECULAR IMAGING